Macromolecules

pubs.acs.org/Macromolecules Article

Crystal Structures of Isotactic and Atactic Poly(1-pentamethylene alcohol)

Kohji Tashiro,* Gina A. Guillory, Stephanie F. Marxsen, Justin G. Kennemur, and Rufina G. Alamo*

Cite This: *Macromolecules* 2023, 56, 5993−6002 Read Online

ACCESS | Metrics & More | Article Recommendations | Supporting Information

ABSTRACT: We have determined the crystal structures of highly regioregular (>97% HT additions) isotactic- and atactic-poly(1-pentamethylene alcohol)s (PPMA, $-[(CH_2)_4CH(OH)]_n-$) by a quantitative analysis of 2-dimensional wide-angle X-ray diffraction data. The unit cell houses two chains in a planar-zigzag conformation, with orthorhombic symmetry and parameters a = 8.637 Å, b = 4.987 Å and c (chain axis) = 12.840 Å for the it-PPMA and a = 8.76 Å, b = 5.06 Å, and c (chain axis) = 12.840 Å for the at-PPMA. The space group is $P2_12_12_1$ for both polymers. The zigzag planes are nearly parallel to the rolled plane of the doubly oriented sample. These regularly packed chains are aggregated in twinned domains having two opposite orientations of the unit cells. In the case of at-PPMA, the random stereochemical positioning of the alcohol pendants results in a more expanded unit cell than the corresponding cell of it-PPMA. Intermolecular hydrogen bonds form along the b axis for both the it- and at-species, the strength of which is slightly different depending on the OH configuration, as judged from infrared spectral information as well as the O···O intermolecular distances.

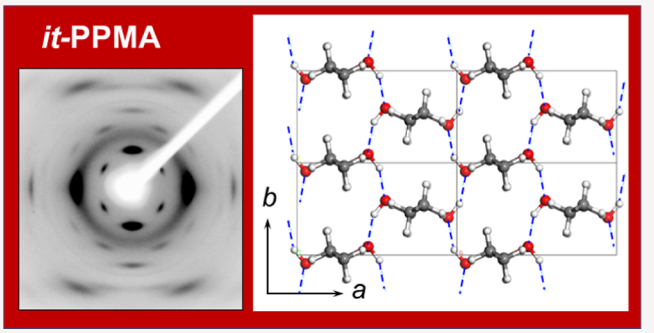

1. INTRODUCTION

Due to strong hydrogen bonding, poly(vinyl alcohol) (PVA, $-[CH_2CH(OH)]_n-$) and ethylene-vinyl alcohol statistical copolymers (EVOH, $-\{[CH_2CH_2]_x\text{-}[CH_2CH(OH)]_y\}_n-$) are extensively used as oxygen barrier packaging materials.[1−7] PVA and EVOH are semicrystalline polymers, and as such, the relation between crystalline structure and properties, including barrier performance, has also been of interest. Because gas molecules diffuse preferentially through the amorphous phase, an increase in the degree of crystallinity (X_c) of the PVA homopolymer, or of the copolymers invariably leads to better barrier properties as shown in earlier and more recent works.[2,5,6]

While PVA is an excellent barrier to oxygen, it is a poor water barrier due to its hydrophilicity.[8] Copolymerization of vinyl alcohol with ethylene results in a decreased X_c and thus an increase in oxygen permeability. However, this is compensated by a significant increase in degradation temperature which helps with melt processing. Furthermore, long ethylene "runs" in the copolymers decrease hydrophilicity and water permeation.[8] Therefore a balance of oxygen and water barrier properties can be targeted from EVOH systems through judicious selection of comonomer composition coupled with X_c. A recent work has demonstrated that such balance could be achieved by precision systems with ethylene backbones and a relatively high content (∼25%) of OH pendants.[9]

Due to the strong correlation between barrier properties and X_c, there has been interest in contrasting the crystalline properties of atactic versus more stereoregular PVA.[10,11] However, despite efforts to increase PVA stereoregularity, the isotacticity remained relatively low, with 78% being the highest reported from NMR calculations based on mm triads.[12−14] Consequently, X_c did not differ much between atactic and isotactic PVA. Moreover, with an increasing fraction of mm triads in the range of 0.14−0.79, the melting temperature and the enthalpy of fusion display a minimum at mm values of 0.4−0.5.[11] The same minimum in thermal properties is found with increasing ethylene content at 40−50 mol % ethylene for a series of EVOH copolymers in a wide range of composition.[15,16]

The crystal structure information is important in the above discussion. The crystal structure of at-PVA was proposed by Bunn in 1948.[17] Two planar-zigzag chains pass through a monoclinic unit cell of the space group $P2_1/m$-C_{2h}. These chains are connected through two types of intermolecular hydrogen bonds in a direction perpendicular to the chain

Received: May 29, 2023
Revised: July 3, 2023
Published: July 24, 2023

https://doi.org/10.1021/acs.macromol.3c01060
Macromolecules 2023, 56, 5993−6002

Scheme 1. Microstructural Comparison of Precise PPMAs Used in This Study to a Typical EVOH Copolymer

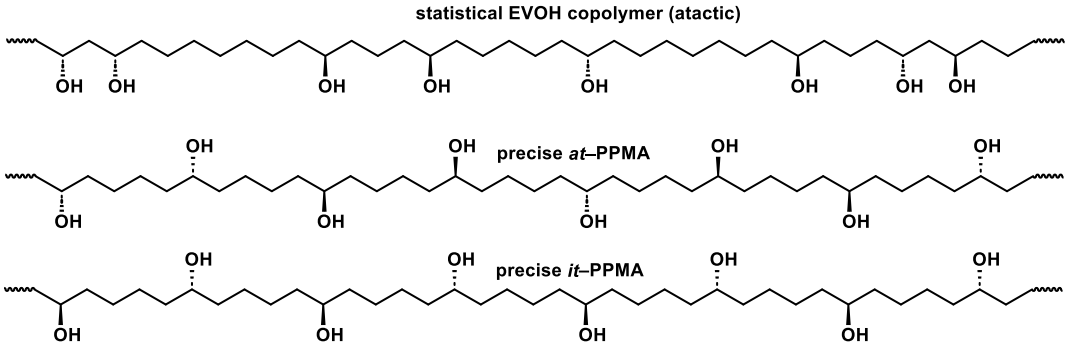

axis.[18] Recently, the crystal structure of at-PVA was refined by the hybridized analysis of wide-angle X-ray and neutron diffraction data, in which the domains composed of Bunn's unit cell structure are aggregated irregularly with a translational slippage along the diagonal direction of the *ab* plane.[19] The crystal structures of a series of EVOH materials were proposed on the basis of the wide-angle X-ray diffraction (WAXD) and Fourier-transform infrared (FTIR) spectroscopy.[20] All of these samples were in the atactic configuration. However, there remains controversy as to if the chain packing at the most fundamental level differs between atactic and isotactic PVA. 2D X-ray fiber patterns and polarized IR spectra of a lowly isotactic PVA inferred a similar unit cell to the refined cell of the atactic PVA but with preferential intramolecular hydrogen bonding instead of the intermolecular hydrogen bonding of the at-PVA crystal structure.[20−22] Further, WAXD of un-oriented and more stereoregular it-PVA obtained by Ohgi and co-workers differed from that of at-PVA and suggested a different crystal structure.[12] Clearly, the difficulty in synthesizing highly stereoregular it-PVA has rendered equivalence of the unit cells of at- and it-PVA inconclusive.

Different from these more-or-less ambiguous PVA relatives, precision systems with an ethylene backbone and OH pendants placed at a precise distance along the chain are of interest, because the ratio between OH/ethylene content can be well controlled while also maintaining high levels of crystallinity. On this path, remarkable progress in ring-opening metathesis polymerization (ROMP) and acyclic diene metathesis polymerization has made it possible to synthesize linear EVOH analogs with OH pendants placed at precise distances along a polyethylene backbone. For example, ROMP of cyclooctene derivatives permits investigation of the importance of precision placement of alcohol pendants by producing one carbinol per every eight backbone carbons in a precise (regiospecific) or purposefully imprecise (regiorandom) fashion.[9] Although both systems are presumably atactic, there were major differences in their properties. The melting point, heat of fusion, and oxygen barrier of the regiospecific polymer were higher than for the regiorandom analog. The regularity of monomer addition in the former also led to relatively sharp WAXD peaks while one broad pattern was observed for the regiorandom.[9]

Using ROMP of trialkylsilyl-protected 2-cyclopentenol, followed by hydrogenation and deprotection, we recently synthesized atactic and isotactic poly(1-pentamethylene alcohol) (PPMA), both with extremely high levels of regioregularity (head to tail addition >97%).[23] The chemical structures are shown in Scheme 1 comparatively with the structure of an ethylene-vinyl alcohol statistical copolymer.

These polymers, which we term at-PPMA and it-PPMA in the present work respectively, are characterized by the precise placement of one alcohol pendant on every fifth backbone carbon with the atactic or isotactic (>90%) configuration and hence offer a higher carbinol/methylene ratio for the balanced barrier properties mentioned above. As described in ref 23, in addition to describing the synthesis in detail, a comparative study of the melting behavior and higher-order structures of the highly stereoregular atactic and isotactic PPMA species was reported.[23] While the T_g of both at-PPMA and it-PPMA is similar, ∼50 °C, the melting temperature (T_m) and X_c changed significantly. For at-PPMA and it-PPMA, T_m = 125 and 190 °C, respectively, while the X_c increased from 0.2 to 0.4.[23] One interesting feature from the comparative work was the effect of tacticity on segmental packing. On the one hand, WAXD patterns of isothermally crystallized at- and it-PMMA are very similar, inferring an equivalent chain packing mode. On the other hand, a lower angle shift of the main diffraction peak in the WAXD pattern of the atactic polymer inferred a more expanded (less dense) crystal lattice than the lattice of the isotactic analog. The densification of the isotactic crystals was attributed to a more efficient intermolecular hydrogen bonding facilitated by the stereoregularity of the alcohols. As inferred from SAXS patterns, although the correlation length between lamellae crystals is longer in at-PPMA, the crystallites are thinner and more defective than the it-PPMA crystals.[23]

The availability of these highly regioregular PPMAs with well-defined atactic and isotactic configurations offers the opportunity for quantitative X-ray analysis of their fiber patterns and thus, enables to elucidate differences, if any, in their crystal structures. We describe these analyses in the present work.

2. EXPERIMENTAL SECTION

2.1. Samples. The methods for synthesizing at-PPMA and it-PPMA were previously reported through regiospecific ROMP of 3-(*tert*-butyldimethylsilyl), TBS, protected 2-cyclopentenol followed by mild hydrogenation of the backbone olefins and quantitative deprotection of the alcohols.[23] The bulky TBS groups serve to promote regioregular (high H−T) propagation of the monomer in addition to providing good solubility of the polymer for characterization prior to deprotection. Due to the unique microstructure of these materials, several potential names are possible. While poly(ethylene-*per*-vinyl alcohol-*per*-methylene) and poly(ethylene-*alt*-vinyl alcohol-*alt*-methylene) are both acceptable, we refer to these materials as PPMA herein for simplicity. Molecular characterization details of the two samples studied here are listed in Table 1. While the at-PPMA is identical to the one previously reported,[23] the it-PPMA

https://doi.org/10.1021/acs.macromol.3c01060
Macromolecules 2023, 56, 5993−6002

Table 1. Molecular Characterization of Atactic and Isotactic PPMA

sample	M_n (kDa)[a]	$Đ$[b]	% HT[c]	T_m (°C)[d]	ΔH_m (J/g)[d]
at-PPMA	410	1.6	99	137	40
it-PPMA	30	1.9	97	183	88

[a]Calculated number average molar mass (M_n) based on size exclusion chromatography (SEC) of the respective TBS-protected version of the polymer and corrected for the quantitative loss of TBS groups. [b]Dispersity ($Đ$) determined by SEC analysis on TBS-protected versions of the polymer. [c]Percentage head−to−tail regioregularity determined by peak deconvolution analysis of methine proton signals from ^{1}H NMR in $CDCl_3$. [d]Melting temperature (T_m), and enthalpy of melting (ΔH_m) determined by differential scanning calorimetry upon second heating at 10 °C min^{-1}.

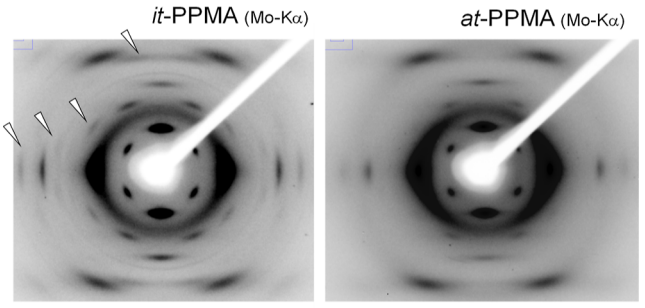

Figure 1. 2D-WAXD patterns measured for the uniaxially oriented it-PPMA and at-PPMA.

was newly synthesized through identical methods. The characterization details are provided in Supporting Information 1. The PVA used for comparative FTIR studies was kindly supplied by Kuraray Co. Ltd., Japan, the degree of polymerization of which was ca. 1700, and the degree of saponification was 99.9%.

PPMA samples were melt-pressed at ca. 20 °C above their melting points and cooled to ambient temperature to make ca. 300 μm thick tapes. The thus-obtained un-oriented tapes were drawn by about 3 times the original length on a hot plate at a preset temperature (it: ca. 150 °C and at: ca. 70 °C). The oriented it-PPMA was fixed strongly by a metal holder and annealed at 160 °C for 1 h in an oil bath. The oriented at-PPMA was annealed at 70 °C for 2 h in the same way. A doubly oriented it-PPMA was prepared by shearing the oriented sample between two metal plates in a direction parallel to the initial drawn axis, followed by the heat treatment at 160 °C for 1 h.

2.2. X-ray Diffraction Measurements. The 2-dimensional WAXD patterns were measured for the oriented samples using a Rigaku X-ray diffractometer (Saturn) equipped with a CCD camera (Saturn 724), with Mo Kα line (0.7107 Å) as incident X-ray beam monochromatized with a confocal mirror. The sample-to-camera distance was corrected using the diffraction peaks of Al powder.

2.3. FTIR Spectral Measurement. The IR spectra were collected using a Thermo Scientific Nicolet iS50 spectrometer equipped with a DTGS KBr detector. The OMNIC software was used for instrument control and peak analysis. The spectrometer was operated in transmission mode within wavenumbers of 4000 and 400 cm^{-1} with 2 cm^{-1} resolution.

2.4. X-ray Data Analysis. The (x, y) positions of the diffraction peaks detected in the 2D-WAXD patterns were read and transformed to the (ξ, ζ) coordinates of the cylindrical coordinate system. The indexing of all the observed peaks and the determination of the unit cell parameters were performed using the thus-estimated (ξ, ζ) data. The diffraction profiles along the individual layer lines were extracted from the 2D WAXD patterns by integrating along the lines.

2.5. Computer Simulations. Crystal structure models were created using the commercial software Cerius^2 (version 4.10, Biovia) with a COMPASS force field.[24] The models were energetically optimized. The 1D and 2D WAXD patterns were calculated using the same software.

Table 2. Lattice Spacings and Indices (it-PPMA)

h	k	l	d(obsd)/Å	d(calc)/Å
2	0	0	4.32	4.32
1	1	0		4.32
3	1	0	2.48	2.49
0	2	0		2.49
4	0	0	2.12	2.16
2	2	0		2.16
5	1	0	1.64	1.63
4	2	0		1.63
1	0	1	7.15	7.17
3	0	1	2.77	2.81
3	2	1	1.92	1.86
0	0	2	6.39	6.42
2	0	2	3.54	3.58
1	1	2		3.58
1	0	3	3.82	3.84
0	0	4	3.18	3.21
1	0	5	2.43	2.46
2	0	5	2.23	2.21
1	1	5	2.23	2.21
3	1	5	1.77	1.79
5	1	5	1.38	1.38
4	2	5		1.38
2	3	5		1.38
0	0	6	2.10	2.14
0	1	7	1.72	1.72
2	0	10	1.23	1.23
1	1	10		1.23

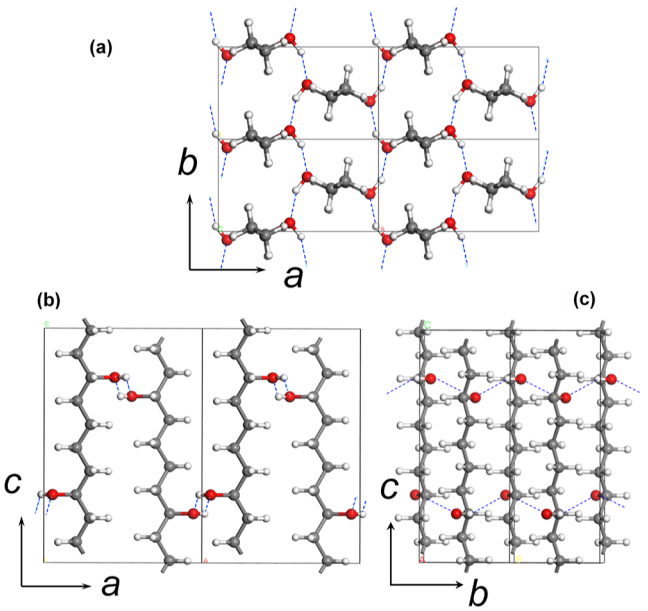

Figure 2. Crystal structure of regularly packed it-PPMA chains. (a) View of the projection on the (ab) plane, (b) view of the projection on the (ac) plane, and (c) view of the projection on the (bc) plane.

https://doi.org/10.1021/acs.macromol.3c01060
Macromolecules 2023, 56, 5993−6002

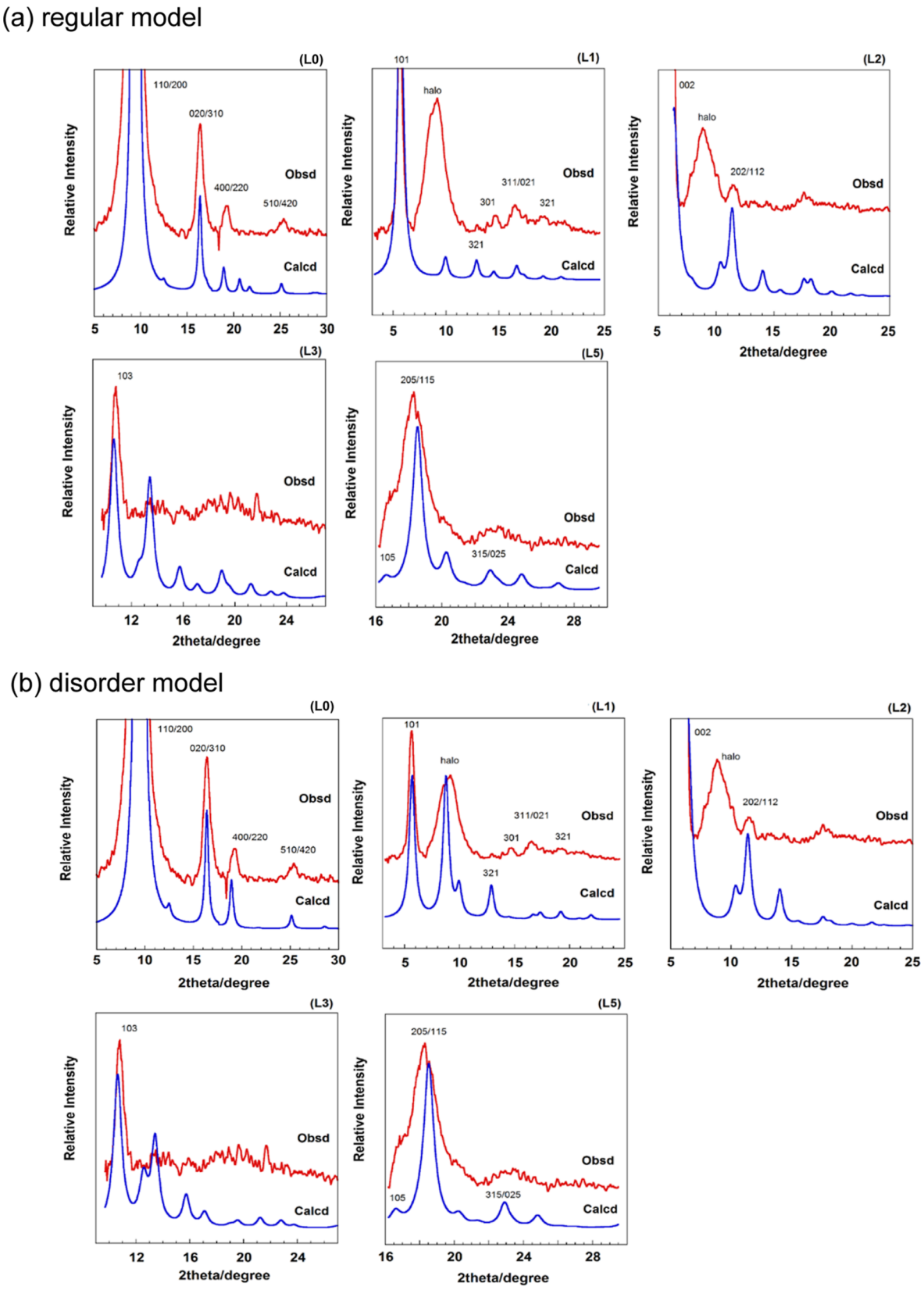

Figure 3. Comparison between the observed (red) and calculated (blue) 1D-diffraction profiles of it-PPMA along the various layer lines: (a) regular structure model and (b) disordered structure model. In the calculation of the diffraction profiles, the crystallite size is 50 Å (//*a*), 50 Å (//*b*), and 50 Å (//*c*), the lattice strain is 0.0 (//*a*), 0.0 (//*b*), 0.0 (//*c*), and the isotropic temperature factor is 10 Å^2. The "halo" peaks come from the scatterings in the amorphous phase (refer to Figure 1).

https://doi.org/10.1021/acs.macromol.3c01060
Macromolecules 2023, 56, 5993−6002

Table 3. Atomic Fractional Coordinates for it-PPMA Crystal[a,b]

atom	X	y	z	atom	x	y	z
C1	0.209	0.040	−0.109	H9(C2)	0.410	0.054	−0.008
C2	0.294	0.956	−0.010	H10(C3)	0.185	0.250	0.089
C3	0.206	0.031	0.089	H11(C3)	0.090	0.935	0.087
C4	0.290	0.952	0.190	H12(C4)	0.306	0.732	0.191
C5	0.204	0.033	0.290	H13(C4)	0.407	0.042	0.190
H6(C1)	0.094	0.947	−0.110	O14(C5)	0.055	0.907	0.290
H7(C1)	0.190	0.259	−0.108	H15(O)	−0.016	0.056	0.291
H8(C2)	0.316	0.738	−0.011	H16(C5)	0.188	0.253	0.290

[a] a = 8.637 Å, b = 4.987 Å, c(chain axis) = 12.840 Å, space group $P2_12_12_1$. [b] The different chain coordinates for the unit cell of a disordered model are generated by rotating the original chains by 180° around the a axis as described in the text.

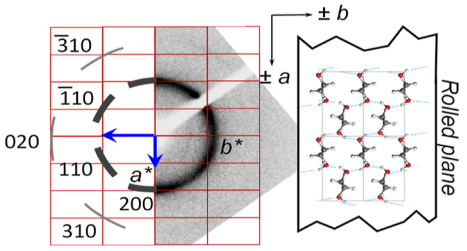

Figure 4. X-ray diffraction pattern measured for the doubly oriented it-PPMA and its indexing. The X-ray beam was incident along the chain axis (end pattern) as shown in the structure model.

3. RESULTS AND DISCUSSION

Figure 1 shows the 2D WAXD patterns measured for it- and at-PPMA samples. The whole X-ray diffraction patterns are quite similar to each other between the it- and at-samples, suggesting essentially the same crystal structure. However, the diffraction peaks are, as a whole, sharper for it-PPMA compared to at-PPMA (see the peaks indicated by arrows for it-PPMA which are almost absent in the at-PPMA). It is perceived that this originates from the difference in the degree of disorder in the crystal structure, as will be discussed in a later section. Initially, we will focus on the chain conformation and packing mode of these unique highly regioregular chains in the unit cell.

3.1. Crystal Structure Analysis of it-PPMA. After accounting for all observed diffraction spots in the 2D WAXD pattern (Figure 1), the most plausible unit cell parameters were determined as

$$a = 8.637\ \text{Å}, \quad b = 4.987\ \text{Å},$$
$$c(\text{chain axis}) = 12.840\ \text{Å}, \quad \alpha = \beta = \gamma = 90^\circ$$

The observed lattice spacings are in good agreement with those calculated using the thus-determined unit cell parameters, as shown in Table 2. The ratio a/b = 1.73 indicates apparently a pseudo-hexagonal unit cell. The indices of the observed diffraction peaks, as listed in Table 2, suggest the systematic extinction rules of $h00$ (h = odd), $0k0$ (k = odd), and $00l$ (l = odd). Then, the unit cell having the orthorhombic symmetry was taken as the first candidate.

The chain conformation can be estimated assuming an *all-trans* sequence of monomeric units. The repeating period of the polyethylene zigzag chain is 2.54 Å and contains two CH_2 units. The period of syndiotactic PVA (*st*-PVA) is 2.55 × 2 Å, containing two monomeric units. Therefore, the effective length of one CH_2 unit is ∼1.27−1.28 Å. The repeating period of PPMA contains two monomeric units; $[(CH_2)_4CH(OH)] \times 2 \approx (CH_2)_{10} \approx 1.28 \times 10 = 12.8$ Å, corresponding very closely to the observed repeating period (c = 12.840 Å). With the above, the c axial length corresponds to the repeating

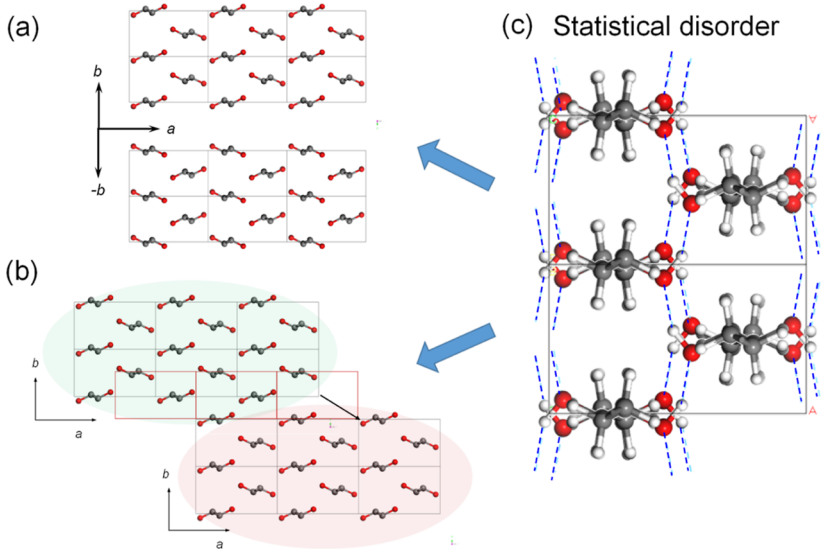

Figure 5. Domain structure models of it-PPMA consisting of (a) unit cells of opposite orientation and (b) unit cells of a diagonal shift in the (ab) plane. (c) The packing disordered structure model build-up by the X-ray coherent domains.

https://doi.org/10.1021/acs.macromol.3c01060
Macromolecules 2023, 56, 5993−6002

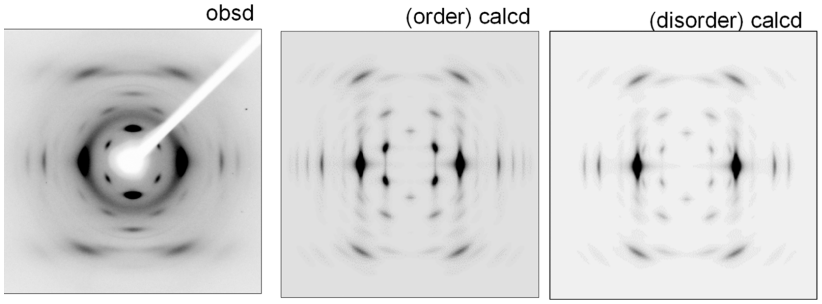

Figure 6. Comparison of the observed 2D WAXD pattern of it-PPMA sample with those calculated for the ordered and disordered models (refer to Figures 2 and 5). The incident X-ray beam is Mo Kα with a wavelength of 0.7107 Å.

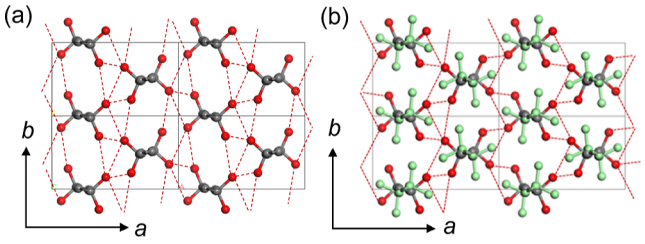

Figure 7. Crystal structure of at-PPMA. (a) Regular chain packing. Unlike it-PPMA, the carbinol stereochemistry is inverted at 50% probability as indicated by red atoms. The H atoms are not shown for simplicity. The hydrogen bonds are formed along the *b* axis as shown in the red dashed lines. (b) The disordered chain packing, where the gray and green atoms represent different chains positioned at one lattice point with different orientations (refer to Figure 5). The green chains are generated by rotating the original gray chains by 180° around the *a* axis.

period of two monomer units along the chain axis with a planar-zigzag conformation. From these considerations, the initial testing model was assumed to consist of 4 asymmetric $[(CH_2)_4CH(OH)]$ units packed in an orthorhombic unit cell with the space group $P2_12_12_1$. The relative positions of the asymmetric units were changed, and the most stereochemically reasonable structure was searched by trial-and-error. The thus-derived structure is shown in Figure 2, where the two zigzag chains are packed in a herringbone mode to maximize the intermolecular hydrogen bonding of O···H···O type along the *b* axis. The model of Figure 2 was refined further to reproduce the observed diffraction profiles along the individual layer lines. A comparison of experimental and computed 1D diffraction profiles is presented in Figure 3a. There is a good agreement for the most intense reflections between observed and calculated patterns. The atomic coordinates of one asymmetric unit are listed in Table 3.

The reliability factor (R factor) is usually calculated as a measure of agreement between observed and calculated diffraction profiles. However, the R factor calculation is omitted here due to large uncertainties in calculating this value from the relatively small number of observed diffraction spots in Figure 1.

As shown in Table 2, the calculated *d* spacings for the (200) and (110) planes of the orthorhombic lattice are equivalent. Hence, it is difficult to know the direction of hydrogen bonds in the anisotropic sample. Then, the initial uniaxially oriented film was subjected to additional orientation by rolling the film in a direction parallel to the initial draw axis. Figure 4 shows the 2D WAXD pattern measured for the doubly oriented it-PPMA sample with the X-ray beam incident along the chain axis. The indexing of the observed diffraction peaks is shown in this figure. The *a* axis, or the averaged plane of the planar-zigzag chains, is found to orient along the rolled plane of the sample. The hydrogen bonds are directed to the *b* axis. This preferential orientation of the zigzag chains along the *a* axis allows us to visualize a possible packing disorder of the zigzag planes that may lead to the observed diffuse spots in Figure 1. One example is illustrated in Figure 5 where we have considered the twin structure or the coexistence of different domains of the same crystal structure. There are several possibilities to create an X-ray coherent domain structure. One possibility is combining the aggregated unit cells with opposite orientation, i.e. differing in 180° rotation of the *b* axis around the *a* axis (Figure 5a). The second possibility is to shift the unit cells by one-half along the diagonal direction of the *ab* plane (Figure 5b). If these domains are X-ray-coherent, the coexistence of such domains would suggest a unit cell structure with disordered packing of the chains (Figure 5c). The 1D diffraction profiles calculated for this disordered model are shown in Figure 3b. At a glance, the calculated diffraction profiles are very similar between the ordered and disordered models. However, judging from the equatorial (L0) and first-layer (L1) line profiles, the agreement between the calculated and observed 1D profiles was improved for the disordered model. The observed and calculated 2D-WAXD patterns of ordered and disordered models are illustrated comparatively in Figure 6. Here, also, the reproduction of the whole observed pattern is closer for the disordered model.

In Figure 6, one notices that the observed meridional diffraction peaks (002, 004, ...) are stronger than the calculated values. This situation is encountered from differences in the crossing degree of the 00*l* reciprocal points with the Ewald sphere.[25] As illustrated in Figure S2-1 of Supporting Information 2, the intersection of the reciprocal lattice point with the Ewald sphere changes depending on the degree of crystallite orientation along the draw direction and/or the broad width of the reciprocal lattice point caused by the small crystallite size. These factors could lead to a higher probability of intersecting the sphere, thus resulting in an apparently strong intensity for the *00l* peaks. This effect has not been taken into account in the calculation of the profiles given in Figure 3.

3.2. Crystal Structure Analysis of at-PPMA. The 2D WAXD pattern of at-PPMA sample (Figure 1b) was analyzed similarly as done above for it-PPMA sample. The resulting unit cell parameters are

https://doi.org/10.1021/acs.macromol.3c01060
Macromolecules 2023, 56, 5993−6002

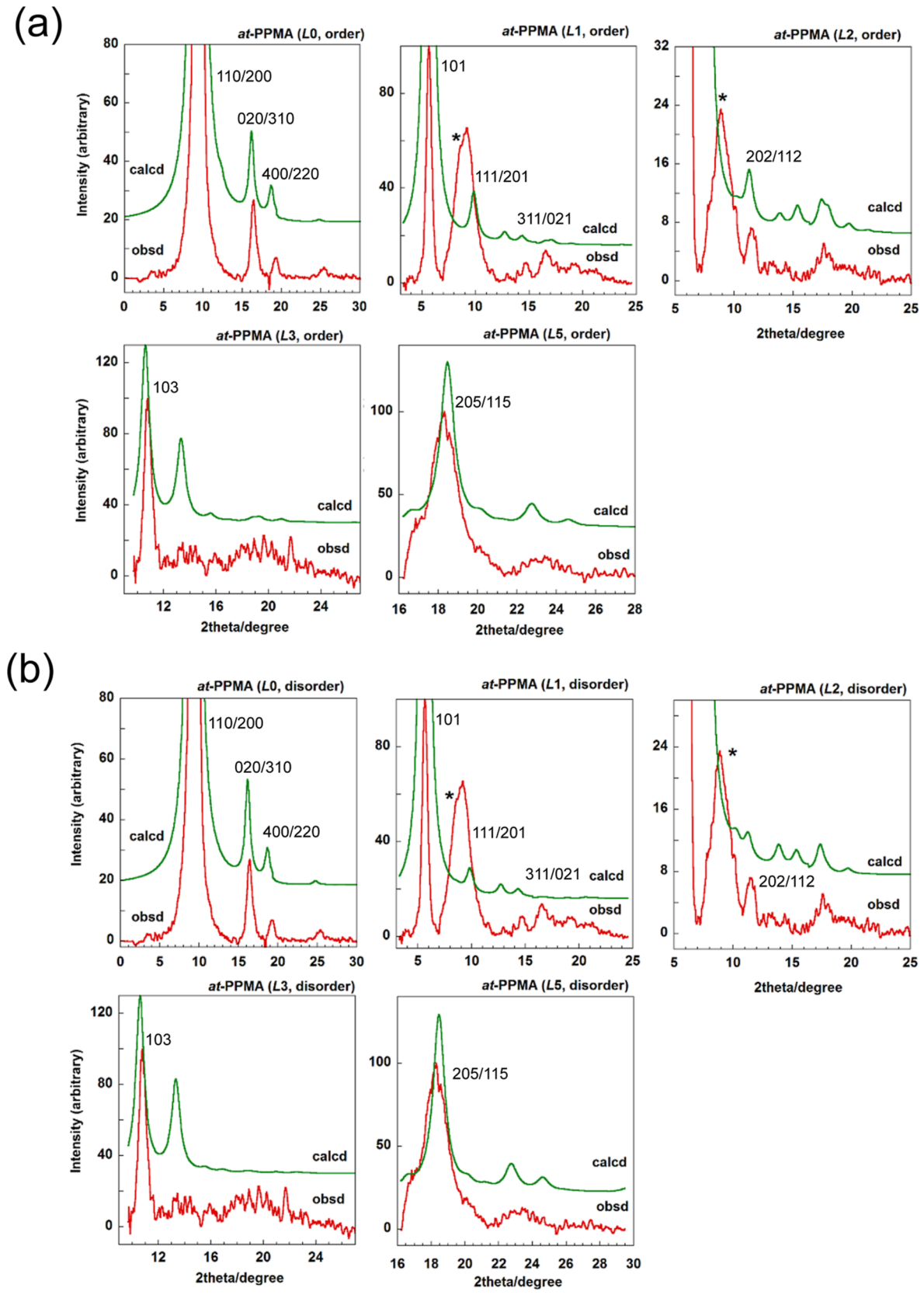

Figure 8. Comparison of observed (red) and calculated (green) diffraction profiles of at-PPMA along the layer lines: (a) regular packing model (Figure 7a), and (b) chain-packing-disordered model (Figure 7b). In the calculation of the diffraction profiles, the crystallite size is 60 Å (//a), 60 Å (//b), and 60 Å (//c), the lattice strain is 0.1 (//a), 0.1 (//b) and 0.5 (//c), and the isotropic temperature factor is 25 Å^2. The peaks with asterisk come from the halo scatterings from the amorphous phase.

https://doi.org/10.1021/acs.macromol.3c01060
Macromolecules 2023, 56, 5993−6002

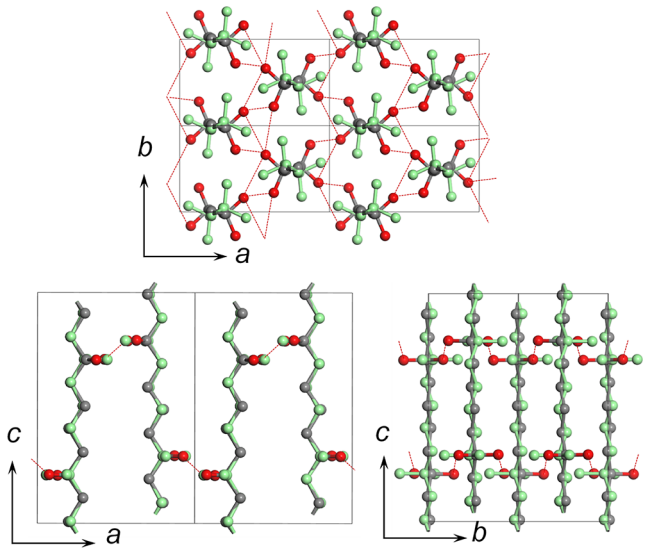

Figure 9. Disordered crystal structure of at-PPMA viewed along the three mutually perpendicular axes (refer to Figure 7b).

$$a = 8.76\ \text{Å}, \quad b = 5.06\ \text{Å}, \quad c(\text{chain axis}) = 12.840\ \text{Å},$$
$$\alpha = \beta = \gamma = 90^\circ$$

The indexing is essentially the same as that for it-PPMA. However, the *a*- and *b*-axial lengths are longer than those of it-PPMA case, thus indicating a more expanded lattice for at-PPMA in agreement with earlier predictions from WAXD patterns of non-oriented specimens.[23] The ratio $a/b = 1.73$ suggests a pseudo-hexagonal packing of the molecular chains. The repeating period is the same as that of it-PPMA, but in modeling the packing structure the stereochemistry of the carbinol is inverted at 50% probability, thus reflecting the atactic configuration. In addition, as introduced for it-PPMA crystal, a disordered aggregation of domains of unit cells was also considered to exist in the at-PPMA crystal. Using the same rationale to introduce disorder in the crystalline arrays of PVA,[19] the at-PPMA packing model of Figure 7a was shifted along the diagonal direction in the *ab* plane (or by 180° rotation around the *a* axis), resulting in the overlap of green and gray chains at 50% probability, as shown in Figure 7b. From the above, the configurationally irregular polymer chains of at-PPMA are packed in disorderly aggregated domains. Such aggregates could explain the diffuse WAXD pattern of at-PPMA seen in Figure 1b.

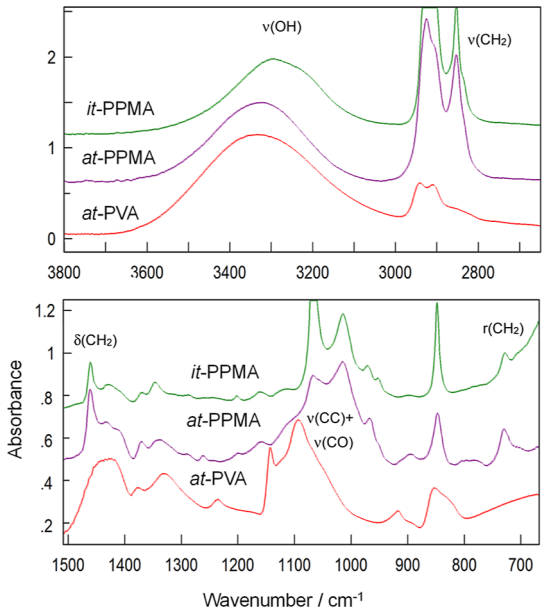

Figure 10. Comparison of FTIR spectra observed for the it-PPMA, *a*t-PPMA, and at-PVA films.

The calculated X-ray diffraction profiles are compared with the observed data in Figure 8. The introduction of chain-packing disorder does not modify the X-ray diffraction profiles drastically, only weak diffraction peaks change their relative intensities (for example, the second-layer line profile). As a final solution, the chain-packing-disordered model (Figure 7b) is adapted here, which is consistent with the disordered model of it-PPMA. The crystal structure of the disordered model viewed along the various crystal axes is given in Figure 9. The atomic coordinates of the regular at-PPMA unit (Figure 7a) are listed in Table 4.

3.3. Intermolecular Hydrogen Bonds. In this section, we discuss hydrogen bond lengths from the crystal structures given above for the novel regioregular atactic and isotactic PPMA in comparison with those given in prior works for at-PVA.[17,19] The O···O distances between neighboring chains are evaluated by the X-ray structure analyses as follows.

it-PPMA 2.86 Å

at-PPMA 2.87 Å, 3.02 Å

at-PVA 2.63 Å, 3.16 Å

Table 4. Atomic Fractional Coordinates for at-PPMA Crystal[a,c]

atom	*x*	*y*	*z*	atom	*x*	*y*	*z*
C1	0.211	0.015	0.610	H11(C5)[b]	0.140	0.232	0.207
C2	0.302	−0.012	0.507	H12(C1)	0.159	0.222	0.614
C3	0.200	0.025	0.410	H13(C1)	0.115	−0.136	0.610
C4	0.290	−0.008	0.308	H14(C2)	0.396	0.143	0.504
C5	0.191	0.025	0.209	H15(C2)	0.356	−0.217	0.504
O6[b]	0.128	0.278	0.207	H16(C3)	0.148	0.232	0.413
O7[b]	0.074	−0.162	0.210	H17(C3)	0.104	−0.128	0.411
H8(O6)[b]	0.213	0.422	0.237	H18(C4)	0.384	0.147	0.304
H9(O7)[b]	−0.021	−0.088	0.259	H19(C4)	0.344	−0.212	0.307
H10(C5)[b]	0.096	−0.128	0.209				

[a] $a = 8.76$ Å, $b = 5.06$ Å, c(chain axis) = 12.840 Å, space group $P2_12_12_1$. [b] Occupancy 0.5. [c] The different chain coordinates for the unit cell of a disordered model are generated by rotating the original chains by 180° around the *a* axis as described in the text.

https://doi.org/10.1021/acs.macromol.3c01060
Macromolecules 2023, 56, 5993−6002

From the above data, we can deduce that the irregular OH positions form two different types of hydrogen bonding in at-PPMA and at-PVA, thus differing from a single H-bonding in the it-PPMA (compare Figures 2 and 9). Such random displacements of the OH groups lead to the observed expansion of the unit cell of at-PPMA. Moreover, a slight increase in the setting angle of the zigzag chains is considered to stabilize the at-PPMA chain packing so that the intermolecular hydrogen bonds are formed effectively.

Figure 10 shows the IR spectra measured for these three samples cooled from the melt at 10 °C/min. Pending detailed normal modes analysis for the spectral data interpretation, we can deduce some important H-bonding features from a comparison of these spectra. (i) In the 3200−3400 cm^{-1} region, the O−H stretching band of it-PPMA is detected at a slightly lower wavenumber compared with the bands of at-PPMA and at-PVA, thus indicating the existence of stronger hydrogen bonds in the crystal lattice of it-PPMA. (As explained in references,[25−27] strong hydrogen bonding of OH···O′ causes the force constant of the O−H bond to become weaker because the O−H bond length becomes longer by the attractive force toward O′ atom, resulting in the shift of OH stretching band to the lower wavenumber side). (ii) In more detail, in the IR spectrum of it-PPMA, the observed OH stretching bands consist of two components at slightly different peak positions of 3300 and 3220 cm^{-1}. The hydrogen bond length is common to all the OH···O pairs. The observed two band components might originate from the correlation splitting of the OH stretching mode [ν(OH)] between the neighboring chains in the unit cell. The detailed (but qualitative) discussion is given in Supporting Information 3. In the case of at-PPMA (and at-PVA), the hydrogen bond lengths are different depending on the directions (see Figure 9 and ref 19). The observed band profile is complicated due to the coupling of the various effects including the different hydrogen bond strengths and the vibrational coupling among the neighboring chains. (iii) The spectral profile in the fingerprint region of 1500−700 cm^{-1} is appreciably different among these three samples. From prior work, the absorbances in the wavenumber range 1150−1100 cm^{-1} are assigned to CC and CO stretching modes.[28] The strong bands of it- and at-PPMA detected in the 1100−1000 cm^{-1} region are also assigned to the skeletal CC stretching bands of a sequence with a finite number of methylene units, $(CH_2)_4$, as well as to the CO stretching band. (iv) The CH_2 rocking [r(CH_2)] bands are located in the 800−700 cm^{-1} region. As it is well known, the 720 cm^{-1} r(CH_2) band of orthorhombic polyethylene crystal, in which the two zigzag chains are packed in a herringbone mode, splits into two components due to non-equivalent vibrational correlation between the two chains.[25,29] As mentioned in (ii), a similar band splitting might be expected for the crystals of at-PPMA and it-PPMA. However, the observed band at 720 cm^{-1} is apparently singlet. The lack of a clear splitting may be attributed to the approximately parallel alignment of neighboring chains despite their herringbone-style packing (Figures 2 and 9). In addition, it might be noticed that the PVA sample having CH_2 units does not give any band at around 700 cm^{-1}. As known in the study of so-called progression bands of a finite methylene sequence $(CH_2)_m$ contained in a series of alkanes and polyethers of zigzag chain conformation, $-[(CH_2)_mO]_n-$, the methylene rocking mode at around 700 cm^{-1} can be detected for the first time when the $(CH_2)_m$ sequence is longer than $m \geq 3$.[30,31] The CH_2 group sandwiched by CHOH units does not satisfy this condition and gives the CH_2 rocking band at around 850 cm^{-1}.[28]

4. CONCLUSIONS

The crystal structures of highly regioregular it- and at-PPMA were determined upon analysis of observed 2-dimensional WAXD patterns of oriented specimens combined with simulation methods. The planar-zigzag chains are packed in orthorhombic unit cells with a slight tilt of the zigzag planes from the *a* axis. The tilting angle differs between it- and at-PPMA for effective hydrogen bonding between neighboring chains. Furthermore, the volume of the unit cell is slightly expanded in the at-PPMA compared with it-species. Disorder between aggregates of unit cells was also considered in the analysis of both types of PPMA and led to slightly better agreement between the observed and calculated 1-D WAXD profiles.

The orthorhombic chain packing mode of these regioregular PPMA species differs from the monoclinic packing of at-PVA and from the packing of random EVOH copolymers. A novel characteristic of the present polymer studied is the presence of a precisely alternating array of alcohol units resulting from the odd-spaced periodicity (every 5th carbon) along the methylene units, which is unlike the even-spaced periodicity of PVA. Hence, these and related systems may offer a better balance between oxygen and water barrier properties through precise control of the ethylene sequence length and tacticity conferred by the carbinol. The correlation between barrier properties and the type of unit cell awaits further studies.

■ ASSOCIATED CONTENT

Supporting Information

The Supporting Information is available free of charge at https://pubs.acs.org/doi/10.1021/acs.macromol.3c01060.

Supporting Information 1. Characterization Details of it-PPMA. Supporting Information 2. Cartoon Depiction of Reciprocal Lattice Point Crossing the Ewald Sphere. Supporting Information 3. Factor Group Analysis of it-PPMA Crystal (PDF)

■ AUTHOR INFORMATION

Corresponding Authors

Rufina G. Alamo − *Department of Chemical and Biomedical Engineering, Florida A&M and Florida State University College of Engineering (FAMU-FSU), Tallahassee, Florida 32310, United States;* orcid.org/0000-0002-3061-499X; Email: alamo@eng.fsu.edu

Kohji Tashiro − *Department of Future Industry-Oriented Basic Science and Materials, Toyota Technological Institute, Nagoya 46808511, Japan; Aichi Synchrotron Radiation Center, Seto 489-0965, Japan;* orcid.org/0000-0002-7543-2778; Email: ktashiro@aichisr.jp

Authors

Gina A. Guillory − *Department of Chemistry and Biochemistry, Florida State University, Tallahassee, Florida 32306, United States*

Stephanie F. Marxsen − *Department of Chemical and Biomedical Engineering, Florida A&M and Florida State University College of Engineering (FAMU-FSU), Tallahassee,*

https://doi.org/10.1021/acs.macromol.3c01060
Macromolecules 2023, 56, 5993−6002

Florida 32310, United States; orcid.org/0000-0002-7766-8768

Justin G. Kennemur − *Department of Chemistry and Biochemistry, Florida State University, Tallahassee, Florida 32306, United States;* orcid.org/0000-0002-2322-0386

Complete contact information is available at: https://pubs.acs.org/10.1021/acs.macromol.3c01060

Notes

The authors declare no competing financial interest.

■ ACKNOWLEDGMENTS

R.G.A. acknowledges funding from the National Science Foundation DMR 2154026, Polymers Program. For the synthesis of these materials, G.A.G. and J.G.K. would like to acknowledge funding from the National Science Foundation, Grant no. 1750852. K.T. wishes to thank the Frontier Research Center for Applied Atomic Sciences, Ibaraki University, for their kind permission for the using of an X-ray diffractometer.

■ REFERENCES

(1) Blackwell, A. L. Ethylene Vinyl Alcohol Resins as a Barrier Material in Multi-Layer Packages. *J. Plast. Film Sheeting* **1985**, *1*, 205−214.
(2) Mokwena, K. K.; Tang, J. Ethylene Vinyl Alcohol: A Review of Barrier Properties for Packaging Shelf Stable Foods. *Crit. Rev. Food Sci. Nutr.* **2012**, *52*, 640−650.
(3) Zhang, Z.; Britt, I. J.; Tung, M. A. Permeation of Oxygen and Water Vapor through EVOH Films as Influenced by Relative Humidity. *J. Appl. Polym. Sci.* **2001**, *82*, 1866−1872.
(4) Muramatsu, M.; Okura, M.; Kuboyama, K.; Ougizawa, T.; Yamamoto, T.; Nishihara, Y.; Saito, Y.; Ito, K.; Hirata, K.; Kobayashi, Y. Oxygen Permeability and Free Volume Hole Size in Ethylene−Vinyl Alcohol Copolymer Film: Temperature and Humidity Dependence. *Radiat. Phys. Chem.* **2003**, *68*, 561−564.
(5) Lagaron, J. M.; Catala, R.; Gavara, R. Structural Characteristics Defining High Barrier Properties in Polymeric Materials. *Mater. Sci. Technol.* **2004**, *20*, 1−7.
(6) Maes, C.; Luyten, W.; Herremans, G.; Peeters, R.; Carleer, R.; Buntinx, M. Recent Updates on the Barrier Properties of Ethylene Vinyl Alcohol Copolymer (EVOH): A Review. *Polym. Rev.* **2018**, *58*, 209−246.
(7) Ito, K.; Saito, Y.; Yamamoto, T.; Ujihira, Y.; Nomura, K. Correlation Study between Oxygen Permeability and Free Volume of Ethylene−Vinyl Alcohol Copolymer through Positronium Lifetime Measurement. *Macromolecules* **2001**, *34*, 6153−6155.
(8) Hodge, R. M.; Edward, G. H.; Simon, G. P. Water Absorption and States of Water in Semicrystalline Poly(Vinyl Alcohol) Films. *Polymer* **1996**, *37*, 1371−1376.
(9) Dingwell, C. E.; Hillmyer, M. A. Regiospecific Poly(ethylene-co-vinyl alcohol) by ROMP of 3-Acetoxycyclooctene and Postpolymerization Modification for Barrier Material Applications. *ACS Appl. Polym. Mater.* **2023**, *5*, 1828−1836.
(10) Horii, F.; Hu, S.; Deguchi, K.; Sugisawa, H.; Ohgi, H.; Sato, T. H CRAMPS Spectra of Poly(vinyl alcohol) Films with Different Tacticities. *Macromolecules* **1996**, *29*, 3330−3331.
(11) Ohgi, H.; Sato, T.; Hu, S.; Horii, F. Highly isotactic poly(vinyl alcohol) derived from tert-butyl vinyl ether. Part IV. Some physical properties, structure and hydrogen bonding of highly isotactic poly(vinyl alcohol) films. *Polymer* **2006**, *47*, 1324−1332.
(12) Ohgi, H.; Sato, T. Preparation of Highly Isotactic Poly(vinyl alcohol). *Macromolecules* **1993**, *26*, 559−560.
(13) Fujii, K. Stereochemistry of poly (vinyl alcohol). *J. Polym. Sci., Part D: Macromol. Rev.* **1971**, *5*, 431−540.
(14) Wu, T. K.; Ovenall, D. W. Proton and Carbon-13 Nuclear Magnetic Resonance Studies of Poly(vinyl alcohol). *Macromolecules* **1973**, *6*, 582−584.
(15) Cerrada, M. L.; Perez, E.; Pereña, J. M.; Benavente, R. Wide-Angle X-Ray Diffraction Study of the Phase Behavior of Vinyl Alcohol−Ethylene Copolymers. *Macromolecules* **1998**, *31*, 2559−2564.
(16) Matsumoto, T.; Nakamae, K.; Ogoshi, N.; Kawasoe, M.; Oka, H. The Crystallinity of Ethylene-Vinyl Alcohol Copolymers. *Kobunshi Kagaku* **1971**, *28*, 610−617.
(17) Bunn, C. W. Crystal Structure of Polyvinyl Alcohol. *Nature* **1948**, *161*, 929−930.
(18) Assender, H. E.; Windle, A. Crystallinity in Poly(vinyl alcohol). 1. An X-ray Diffraction Study of Atactic PVOH. *Polymer* **1998**, *39*, 4295−4302.
(19) Tashiro, K.; Kusaka, K.; Yamamoto, H.; Hanesaka, M. Introduction of Disorder in the Crystal Structures of Atactic Poly(vinyl Alcohol) and Its Iodine Complex To Solve a Dilemma between X-ray and Neutron Diffraction Data Analyses. *Macromolecules* **2020**, *53*, 6656−6671.
(20) Takahashi, M.; Tashiro, K.; Amiya, S. Crystal Structure of Ethylene−Vinyl Alcohol Copolymers. *Macromolecules* **1999**, *32*, 5860−5871.
(21) Murahashi, S.; Yuki, H.; Sano, T.; Yonemura, U.; Chatani, Y. Isotactic Polyvinyl Alcohol. *J. Polym. Sci., Polym. Lett. Ed.* **1962**, *62*, S77−S81.
(22) Fujii, K.; Mochizuki, T.; Imoto, S.; Ukida, J.; Matsumoto, M. Investigation of the stereoregularity of poly(vinyl alcohol). *J. Polym. Sci., Polym. Chem. Ed.* **1964**, *2*, 2327−2347.
(23) Guillory, G. A.; Marxsen, S. F.; Alamo, R. G.; Kennemur, J. G. Precise Isotactic or Atactic Pendant Alcohols on a Polyethylene Backbone at Every Fifth Carbon: Synthesis, Crystallization, and Thermal Properties. *Macromolecules* **2022**, *55*, 6841−6851.
(24) Sun, H. COMPASS: An *ab* Initio Force-Field Optimized for Condensed-Phase Applications - Overview with Details on Alkane and Benzene Compounds. *J. Phys. Chem. B* **1998**, *102*, 7338−7364.
(25) Tashiro, K. *Structural Science of Crystalline Polymers*; Springer Nature: Singapore, 2022.
(26) Choperena, A.; Painter, P. Hydrogen Bonding in Polymers: Effect of Temperature on the OH Stretching Bands of Poly(vinylphenol). *Macromolecules* **2009**, *42*, 6159−6165.
(27) De Ninno, A.; Del Giudice, E.; Gamberale, L.; Congiu, C. A. The Structure of Liquid Water Emerging from the Vibrational Spectroscopy: Interpretation with QED Theory. *Water* **2013**, *6*, 13−25.
(28) Tashiro, K.; Kobayashi, M.; Tadokoro, H. Polarized Raman Spectra of Doubly Oriented Poly(vinyl alcohol). *Polym. Bull.* **1978**, *1*, 61−66.
(29) Li, H.-W.; Strauss, H. L.; Snyder, R. G. Differences in the IR Methylene Rocking Bands between the Crystalline Fatty Acids and N-Alkanes: Frequencies, Intensities, and Correlation Splitting. *J. Phys. Chem. A* **2004**, *108*, 6629−6642.
(30) Makino, D.; Kobayashi, M.; Tadokoro, H. Structural studies of polyethers $[(CH_2)_mO]n$. XI. Skeletal vibrations of planar zigzag polyethers. *Spectrochim. Acta, Part A* **1975**, *31*, 1481−1495.
(31) Tashiro, K.; Tadokoro, H. Vibrational Spectra of Planar-zigzag Poly(ethylene Oxide). *Rep. Progr. Polym. Phys. Jpn.* **1978**, *21*, 417−420.